JOURNAL OF SYNCHROTRON RADIATION
ISSN 1600-5775

Transmission of an X-ray beam through a two-dimensional photonic crystal and the Talbot effect

V. G. Kohn*

National Research Centre 'Kurchatov Institute', Kurchatov Square 1, 123182 Moscow, Russia.
*Correspondence e-mail: kohnvict@yandex.ru

Received 30 August 2017
Accepted 30 December 2017

Edited by A. Momose, Tohoku University, Japan

Keywords: X-ray transmission; two-dimensional photonic crystal; Talbot effect; computer simulations; iterative algorithm.

Results of computer simulations of the transmission of an X-ray beam through a two-dimensional photonic crystal as well as the propagation of an X-ray beam in free space behind the photonic crystal are reported. The photonic crystal consists of a square lattice of silicon cylinders of diameter 0.5 μm. The amount of matter in the path of the X-ray beam rapidly decreases at the sides of the cylinder projections. Therefore the transmission is localized near the boundaries, and appears like a channeling effect. The iterative method of computer simulations is applied. This method is similar to the multi-slice method that is widely used in electron microscopy. It allows a solution to be obtained with acceptable accuracy. A peculiarity in the intensity distribution inside the Talbot period z_T in free space was found when the intensity is approximately equal to the initial value at a distance $0.46z_T$, and it is shifted by half a period at distance $0.5z_T$. The reason for this effect is the existence of a periodic phase of the wavefunction of radiation inside the intensity peaks. Simulations with zero phase do not show this effect. Symmetry rules for the Talbot effect are discussed.

1. Introduction

Photonic crystals are known to be some of the most promising systems for many applications using visible light (Klimonsky *et al.*, 2011). They have a structure that causes periodic modulation of the dielectric function (refractive index) when the period is comparable with the wavelength of light. Such a periodicity opens the possibility of strong Bragg diffraction of light similar to the Bragg diffraction of X-rays in single crystals (Authier, 2005). As a result, photonic energy bands arise, similar to the electronic energy bands in semiconductors, which leads to filtering of the transmission and reflection of light.

It is known that opals are an example of natural three-dimensional photonic crystals. They consist of $SiO_2{\cdot}nH_2O$ silica globules ordered in a lattice. Artificial opals are usually created in the process of self-assembly of colloid particles like SiO_2 spheres on a vertical surface (Klimonsky *et al.*, 2011). The main problem with such a technique is that it is impossible to create photonic crystals without defects in their structure.

Other techniques allow the creation of one-dimensional or two-dimensional artificial photonic crystals. One-dimensional photonic crystals are known as multilayers. They are created by different deposition techniques and are widely used as mirrors for ultraviolet and soft X-ray radiation (see, for example, Macquart *et al.*, 1991). Two-dimensional photonic crystals are prepared by means of microfabrication techniques on Si surfaces including electron-beam lithography, anisotropic deep plasma etching, LIGA technology and so on.

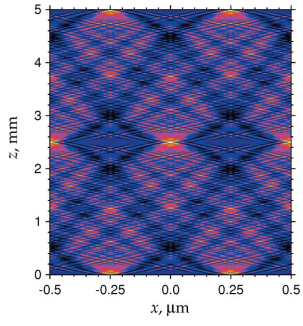

The microfabrication technique allows the creation of a high-quality periodic structure which is free of defects and has sharp boundaries of the composing elements. An example of such a structure is given in Fig. 1, which shows a set of cylinders that form a two-dimensional lattice with a square unit cell having one cylinder inside itself. In terms of crystallography the unit cell has a basis consisting of two elements located at the beginning and at the centre of the unit cell. Fig. 1(*a*) shows a view from the top, while Fig. 1(*b*) shows a three-dimensional image.

Hard X-ray radiation with photon energy E of $\sim$10 keV and higher (wavelength λ of $\sim$0.1 nm and lower) can be used as a diagnostic of photonic crystal structure by means of applying several coherent scattering techniques developed at third-generation synchrotron radiation sources. One of them is the method of small-angle X-ray diffraction which allows one to detect the structure of diffraction spots from a small region of a crystal over a large distance (see, for example, Gulden *et al.*, 2010).

A very promising technique is based on the use of a compound refractive lens (CRL) (Snigirev *et al.*, 1996; Lengeler *et al.*, 1999; Kohn, 2002, 2003). First of all, high-resolution X-ray diffraction can be used at the focus of the CRL at a small distance from the CRL (Kohn *et al.*, 2003; Drakopoulos *et al.*, 2005). Secondly, a high-resolution X-ray microscopy technique has been developed which allows imaging of mesoscopically structured materials. This technique was applied for imaging natural and synthetic opals, inverted photonic crystals and colloidal goethite board-like particles (Bosak *et al.*, 2010; Snigireva & Snigirev, 2013; Meijer *et al.*, 2012; Byelov *et al.*, 2013).

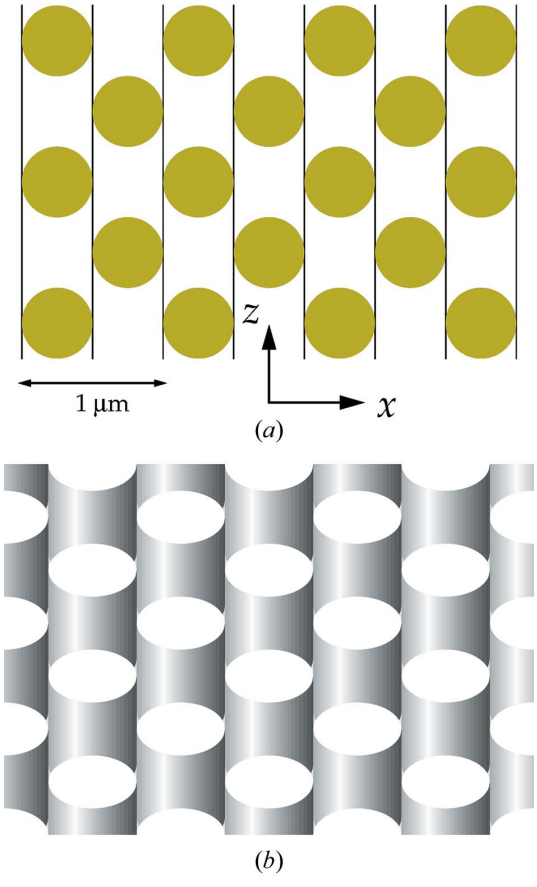

Figure 1
Structure of the two-dimensional photonic crystal used here in the computer simulations. (*a*) View from the top and (*b*) the three-dimensional picture.

On the other hand, a perfect two-dimensional photonic crystal can be used as a new device which is able to modify a coherent homogeneous X-ray beam to a new form of periodic beam structure with a small period. Such a beam can produce an interference image which can be translated in space due to the Talbot effect (Talbot, 1836).

Up to now there have been problems theoretically understanding the process of transmission of a hard X-ray beam through a photonic crystal. The well known theory of phase contrast imaging (Snigirev *et al.*, 1995; Kohn *et al.*, 2010) is not valid because of the strong variation of the phase with a small period for a relatively thick crystal. The kinematic X-ray diffraction theory (Authier, 2005) is not valid because of strong scattering by each element of the structure. The theory of dynamic multiple diffraction is very difficult to realize.

In recent works (Kohn & Tsvigun, 2014; Kohn *et al.*, 2014) an iterative approach based on recurrence relations has been proposed. It is similar to the multi-slice method used in the theory of transmission electron microscopy [see Goodman & Moodie (1974), and references therein], but not entirely. Our method is valid only for periodic systems, *i.e.* for the case where the region of three periods can be calculated in each iteration and the side periods are improved to be equal to the central period. This method was applied to three-dimensional photonic crystals. In this work we apply the same approach to the two-dimensional photonic crystal shown in Fig. 1 for a special orientation of the crystal relative to the beam direction which is shown in Fig. 1(*a*) as the z-axis.

This case is of interest due to the existence of the channeling effect for part of the X-ray beam. A profile of thickness t of Si matter averaged over a period along the beam direction is shown in Fig. 2. The argument is the transverse coordinate x. It shows two minima on the x-axis at the boundaries of the cylinders. These minima have a square-root dependence. It is known that for the focusing lens the minimum has a parabolic profile.

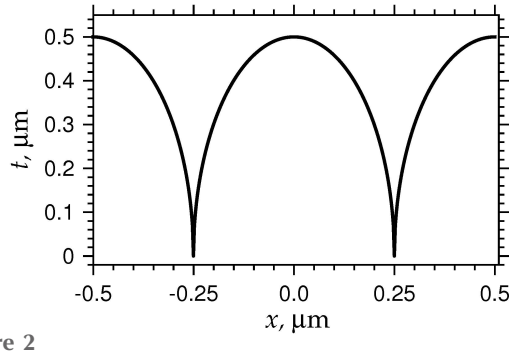

Figure 2
A profile of thickness t of Si matter averaged over a period along the beam direction.

The square-root profile cannot focus the whole beam, but focusing some part of the rays is possible. In any case, the main intensity of the beam can transmit through just these minima while the other parts of the matter profile will absorb the radiation completely. At the exit of the photonic crystal the intensity of the radiation will be strongly modulated with a period of $d = 0.5$ µm although the true period of the structure is 1 µm.

In a further propagation of the modulated beam in free space the Talbot effect with period $z_T = 2d^2/\lambda$ occurs but with an unusual intensity behavior inside the Talbot period. In particular, our calculations do not show the fractional or fractal Talbot effect which was discussed by Berry & Klein (1996). The reason for this is that the phase of the wavefunction inside the peaks is not constant. We have discovered the effect of shifting the intensity peaks by half a period within a very small distance interval.

2. The method of computer simulations

In this work we use the same method of computer simulations as in our previous papers (Kohn & Tsvigun, 2014; Kohn *et al.*, 2014) for three-dimensional photonic crystals. Below we briefly describe the method for the case of a two-dimensional photonic crystal. A variation in the Si matter density occurs in the (x, z) plane as shown in Fig. 1. We consider a crystal orientation such that the X-ray beam propagates along the z-axis.

We search for a solution of the Maxwell equation for the electric field of the radiation in the form

$$E(x, z, t) = \exp(ikz - i\omega t)\, A(x, z). \tag{1}$$

Here $k = \omega/c = 2\pi/\lambda$ is the wavenumber, ω is the frequency of radiation, c is the speed of light, λ is the wavelength and $A(x, z)$ is a slowly varying function which depends on ω where ω is an external parameter. In the paraxial approximation we can neglect the second derivative of A on z and write the equation for A in the form

$$\frac{\partial A}{\partial z} = -ik\eta\, \rho(x, z)\, A + \frac{i}{2k}\frac{\partial^2 A}{\partial x^2}. \tag{2}$$

Here $\eta = \delta - i\beta = 1 - n = -\chi/2$ where n is the complex refractive index of Si matter, $\chi = \varepsilon - 1$ is the susceptibility of the matter and ε is the dielectric function. We consider elastic scattering of the monochromatic radiation and therefore ω is a constant parameter.

The function $\rho(x, z)$ is equal to 1 at a point inside the matter, and 0 at a point in free space. This function describes the structure of a two-dimensional photonic crystal, and can be rather complicated. In our case the photonic crystal consists of cylinders of diameter $d = 0.5$ µm. For the sake of simplicity we begin with a plane wave at the entrance surface of the crystal, $z = 0$, and assume that $A(x, 0) = A_0(x) = 1$.

Since the photonic crystal has a periodic structure we will search for the solution of equation (2) by means of an iterative method. Let us assume that we know the solution $A_n(x)$ after a passage of $n = 2k$ rows of cylinders where k is an integer. We note that one row of cylinders will disturb the wavefunction weakly. We will take this into account by means of a two-step process.

In the first step we neglect the second term on the right-hand side of equation (2) and obtain the new function

$$B_n(x) = A_n(x)\, C_1(x), \quad C_1(x) = \exp\bigl[-ik\eta\, t_1(x)\bigr], \tag{3}$$

where

$$t_1(x) = \int_0^d \mathrm{d}z\, \rho_1(x, z). \tag{4}$$

Here, $t_1(x)$ is a periodic function with period $2d$. According to Fig. 1 we have

$$\begin{aligned} t_1 &= 0 && \text{for } |x| < R, \\ t_1 &= d\bigl[1 - (x - d)^2/R^2\bigr]^{1/2} && \text{for } |x - d| < R, \end{aligned} \tag{5}$$

where $R = d/2$ is the cylinder radius. This approximation corresponds to the phase contrast approach, and it is correct for one row of cylinders.

In the second step we neglect the first term on the right-hand side of equation (2) and obtain

$$A_{n+1}(x) = \int \mathrm{d}x_1\, P(x - x_1, d)\, B_n(x_1), \tag{6}$$

where

$$P(x, z) = \frac{1}{(i\lambda z)^{1/2}} \exp\left(i\pi\, \frac{x^2}{\lambda z}\right) \tag{7}$$

is the Fresnel propagator. This step allows us to take into account the thickness of the photonic crystal which can be quite large.

The next row of cylinders has another structure. This is why we need to take it into account by means of the same process but with a different phase factor,

$$B_{n+1}(x) = A_{n+1}(x)\, C_2(x), \quad C_2(x) = \exp\bigl[-ik\eta t_2(x)\bigr], \tag{8}$$

where

$$t_2(x) = \int_0^d \mathrm{d}z\, \rho_2(x, z). \tag{9}$$

Now, according to Fig. 1 we have

$$\begin{aligned} t_2 &= d(1 - x^2/R^2)^{1/2} && \text{for } |x| < R, \\ t_2 &= 0 && \text{for } |x - d| < R. \end{aligned} \tag{10}$$

Finally we obtain

$$A_{n+2}(x) = \int \mathrm{d}x_1\, P(x - x_1, d)\, B_{n+1}(x_1). \tag{11}$$

The subsequent rows of the photonic crystal have the same structure. We can replace the index $n + 2$ by n and repeat equations (3)–(11) and so on. We would like to consider an infinitely wide photonic crystal, but we cannot calculate the convolution in equations (6) and (11) for infinite limits. On the other hand, the Fresnel propagator oscillates with a small period for a small distance d. We can calculate the convolution by means of the fast Fourier transformation procedure, and we need to use a rather small step in the set of points.

We have solved this problem as described below. The calculations were performed in an interval of 3 μm with the number of points 16384 = 2^{14}. This interval contains three large periods of 1 μm. This is equivalent to a situation where a slit of width 3 μm is located in front of the photonic crystal. It is known that, at a small distance, due to diffraction of radiation on a slit, the part near the boundaries is strongly disturbed while the central part remains unchanged. In other words, the Fresnel propagator at small longitudinal distance has a small size for the first Fresnel zone and any local change of the function $B(x)$ can influence the function $A(x)$ within a small region.

This is valid for one iteration, but it is not valid for many iterations because each new iteration increases the size of the region of influence. To eliminate the influence of the boundaries we have applied a special numerical procedure in each iteration which takes the central period of the function $A(x)$ and improves the left and right periods according to a property of the periodicity of the solution for infinite photonic crystals. Such a procedure allows one to obtain a solution with sufficient accuracy for a crystal of rather large thickness.

We note that there is an alternative iteration process when

$$B_n(x) = A_n(x)\, C_1(x)\, C_2(x) \tag{12}$$

and

$$A_{n+2}(x) = \int \mathrm{d}x_1\, P(x - x_1, 2d)\, B_n(x_1). \tag{13}$$

This second process is faster than the first process but has a smaller accuracy. Nevertheless, we have obtained the same results in our calculations by both processes. This fact can be considered as a way to control the accuracy of the simulations.

In the second iterative process the solution has a transverse period of d from the beginning. The function $t(x) = t_1(x) + t_2(x)$ is shown in Fig. 2. In the first iterative process such a periodicity arises after several pairs of rows. We used the first approach to obtain the wavefunction of radiation at the exit surface of a photonic crystal of arbitrary thickness.

The next task is the calculation of wavefield propagation in air behind the photonic crystal. For an infinitely wide crystal this wavefield stays periodic at all distances. Therefore we can use the same set of points and the iterative process based on the recurrence relation

$$A(x, z + z_0) = \int \mathrm{d}x_1\, P(x - x_1, z_0)\, A(x_1, z) \tag{14}$$

with some constant distance z_0 which now can be as large as possible without causing destruction of the central period of the considered region. At each step the central period was used by us to improve the left and right periods. Sometimes it is useful to apply a small value of z_0 to obtain a detailed picture of the intensity transformation in free space with increasing distance.

3. Results for a photonic crystal

Fig. 3 shows the calculated intensity of radiation $I(x, z) = |A(x, z)|^2$ inside the Si photonic crystal in the form a color map for a photon energy of 12.4 keV (wavelength of 0.1 nm). The

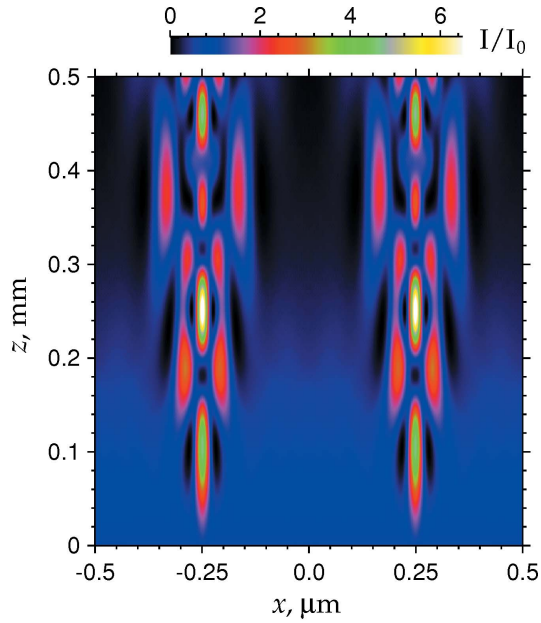

Figure 3
X-ray beam intensity distribution inside the photonic crystal.

refraction parameters $\delta = 3.166 \times 10^{-6}$ and $\beta = 3.155 \times 10^{-8}$ can be obtained by means of an online program (Kohn, 2013). It is assumed that the intensity of the incident radiation $I_0 = 1$. The central period of the photonic crystal including the two boundaries between the cylinders is shown. In reality the period of the intensity is twice as small and it is equal to d = 0.5 μm. We present the intensity profiles $I_n(x)$ after a transmission of 1001 rows of cylinders along the z-axis which were calculated on each iteration. Therefore the maximum thickness of the photonic crystal is equal to 0.5005 mm.

The relative intensity was found to be maximum at a thickness of 0.25 mm with a value 7.194. Since the peak is rather sharp, the maximum value of contrast in Fig. 3 is equal to 6.5. The simulations reveal that the considered photonic crystal is able to focus an X-ray beam by increasing the intensity by up to seven times. The focusing effect arises periodically with various periods and with different maximum values.

The first peak arises at a thickness of 0.1 mm without side peaks. The next peak can be accompanied by small side peaks. For some thicknesses there are several small peaks without a central large peak. The mean intensity decreases with increasing thickness due to absorption in the silicon matter. Fig. 4 shows curves for both the maximum value of the intensity (red curve, left-hand axis) and the mean value of the intensity (blue curve, right-hand axis). Here an interval of thicknesses up to 1.5 mm is shown that is three times larger than in Fig. 3.

One can see that the intensity of the X-ray beam becomes more localized when the peak arises and less localized when the peak is absent. However, for all thicknesses the X-ray radiation is localized within the channel between the boundaries of the cylinders. Sharp changes of the derivative of the maximum intensity function are due to a change in peak when

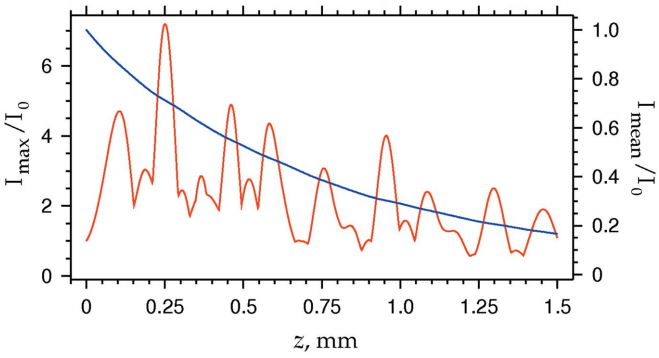

Figure 4
Dependence of the maximum value of the X-ray beam intensity (red curve, left-hand axis) and mean value (blue curve, right-hand axis) on the thickness of the photonic crystal.

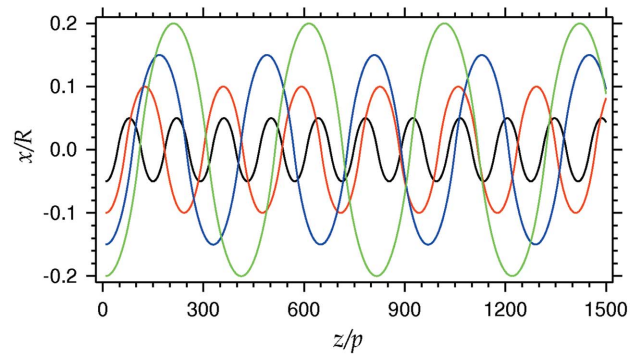

Figure 5
Ray trajectories in the geometrical optics approximation. Four lines with various initial positions are drawn with various colors to better distinguish them.

the intensity value of the new peak becomes greater than the intensity value of the preceding peak. Each time the curve shows the peak with a maximum intensity value.

To understand the channeling effect it is useful to consider ray trajectories according to a geometrical optics approximation. An accurate calculation can be performed by considering the refraction condition on each boundary of the cylinders, but it is rather complicated. Instead we consider the integral (13) after substituting (12). According to the stationary phase method the main contribution to the point x at the layer $n+2$ is obtained from the point x_1 at the layer n where

$$\alpha = \frac{x - x_1}{p} = \frac{\mathrm{d}\varphi_n(x_1)}{k\,\mathrm{d}x} + \frac{\mathrm{d}\varphi(x_1)}{k\,\mathrm{d}x}. \qquad (15)$$

Here, $p = 2d$, $\varphi_n(x)$ is the phase of $A_n(x)$, $\varphi(x) = -k\delta t(x)$ and α is the angle between the ray trajectory and the optical axis.

Then the derivative of α can be calculated as the ratio of the change in α after a passage of one period p and p

$$\frac{\Delta\alpha}{p} = \frac{\mathrm{d}\alpha}{\mathrm{d}z} = \frac{\mathrm{d}\varphi}{pk\,\mathrm{d}x} = -\delta\,\frac{\mathrm{d}t(x)}{p\,\mathrm{d}x}. \qquad (16)$$

We are interested in the ray trajectories near the boundaries of the cylinders. Let this point be the origin on the x-axis. Then we have

$$\frac{\mathrm{d}t(x)}{p\,\mathrm{d}x} = \frac{(2R)^{1/2}}{p}\,\frac{|x|^{1/2}}{x}\left(1 - \frac{|x|}{2R}\right)^{-1/2}\left(1 - \frac{|x|}{R}\right). \qquad (17)$$

It is evident that $\mathrm{d}x/\mathrm{d}z = \alpha$. Then we eliminate a singularity in equation (17), introduce dimensionless variables $s = x/R$ and $n = z/p$, and obtain the following equation for the ray trajectory in the case of an incident plane wave,

$$\frac{\mathrm{d}^2 s}{\mathrm{d}n^2} = -u(s), \qquad \frac{\mathrm{d}s(0)}{\mathrm{d}n} = 0, \qquad s(0) = s_0, \qquad (18)$$

where

$$u(s) = (32)^{1/2}\,\delta\,\frac{s|s|^{1/2}}{(s^2 + a^2)}\left(1 - \frac{|s|}{2}\right)^{-1/2}(1 - |s|). \qquad (19)$$

Here, a is a small parameter which is necessary for computer calculations without a singularity. In reality the approach of ray trajectories is not valid near the point $x = 0$ where the ray inclination is very large. It may be large but finite.

Equation (18) is similar to the equation for a pendulum of special structure. The ray trajectories depend on a point at the entrance surface of the photonic crystal. They are periodical with various periods for different points and symmetrical. Fig. 5 shows four trajectories as a solution of equation (18). The trajectories can intersect and interfere. However, the result of the interference depends on the phases and amplitudes of the fields coming along the different trajectories. We note that in the case of a CRL all trajectories have the same period.

4. The Talbot effect and the peculiarities of wave propagation in free space

We consider a photonic crystal of thickness 0.25 mm for which the intensity distribution of the X-ray beam at the exit surface has the most high peaks, and calculate the propagation of such a beam in free space behind the crystal. It is sufficient to calculate the distance interval from zero to $z_T = 5$ mm because the distribution is repeated periodically with a period z_T.

Fig. 6 shows the calculated intensity distribution as a color map. The maximum value at the centre of a sharp peak is equal to 7.2 but we show the contrast within the interval from zero to 4.5 to reveal the symmetry of distribution. The dependence of the maximum value of intensity on the distance is shown in Fig. 7. We note that the mean values are the same for all distances. The symmetry shown in Fig. 6 is not high compared with images calculated for a periodical slit system (which can be seen, for example, on Wikipedia), and therefore it is necessary to analyse the properties of wave propagation in free space.

A periodic wavefunction with period p for $z = 0$ can be represented as a Fourier series,

$$\psi(x, 0) = \sum_m C_m \exp(iq_m x). \qquad (20)$$

Here, C_m are the coefficients of the Fourier image of the wavefunction, and $q_m = 2\pi m/p$. To calculate the wavefunction

at distance z it is sufficient to multiply the coefficients C_m on the Fourier image of the Fresnel propagator,

$$P(q_m, z) = \exp\left(-i\,\frac{\lambda z}{4\pi} q_m^2\right) = \exp\left(-i\pi\lambda z\,\frac{m^2}{p^2}\right). \quad (21)$$

As a result we have

$$\psi(x, z) = \sum_m C_m \exp(i2\pi m x/p - i\pi\lambda z m^2/p^2). \quad (22)$$

Since m is an integer, it is easy to find that the additional phase is equal to $2\pi k$ with k being an integer if $z = nz_T$, where $z_T = 2p^2/\lambda$ is the Talbot distance. Therefore we obtain the first Talbot rule (Talbot, 1836),

$$\psi(x, z_T + z) = \psi(x, z). \quad (23)$$

Fig. 6 shows this rule in terms of the intensity but it is a property of the wavefunction.

Let us consider the second Talbot rule. If $z = z_T/2$, then $P(q_m, z_T/2) = \exp(-i\pi m^2)$. It is known that the square of even integers is even, and that of odd integers is odd. Therefore, $P(q_m, z_T/2)$ is equal to 1 for even m and to -1 for odd m. This can be written as $P(q_m, z_T/2) = \exp(-i\pi m)$. Then we obtain the second rule (Berry & Bodenschatz, 1999),

$$\psi(x, z_T/2 + z) = \psi(x - p/2, z). \quad (24)$$

This property of the symmetry can be seen in Fig. 6.

It is easy to verify that the symmetric wavefunction stays symmetric for all distances. Additional properties of the Talbot picture are usually derived for particular cases. For example,

$$\psi(x, z_T - z) = \sum_m C_m \exp(i2\pi m x/p + i\pi\lambda z m^2/p^2). \quad (25)$$

If the coefficients C_m are real values then

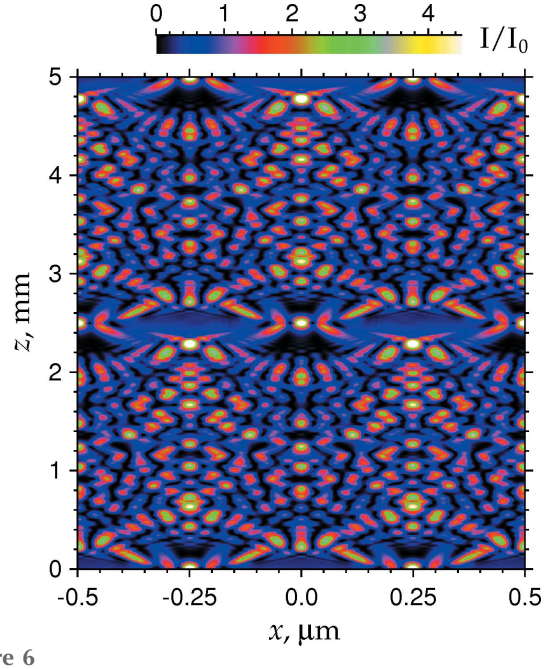

Figure 6
X-ray beam intensity distribution behind the photonic crystal within the Talbot period.

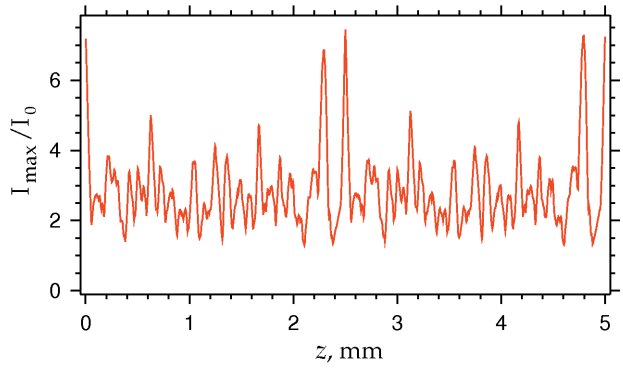

Figure 7
Dependence of the maximum value of the X-ray beam intensity on distance behind the photonic crystal.

$$\psi(x, z_T - z) = \psi^*(-x, z) \quad (26)$$

and we obtain a new symmetry property for the intensity,

$$I(x, z_T - z) = I(-x, z). \quad (27)$$

For a symmetric wavefunction this property becomes simpler,

$$I(x, z_T - z) = I(x, z). \quad (28)$$

One can see that Fig. 6 does not reveal this property. Moreover, a distribution with strong peaks at a distance of 2.3 mm becomes shifted by half a period at a distance of 2.5 mm. We note that the intensity distribution at a distance of 2.3 mm is close to the initial distribution at zero distance with approximately the same peak height, as can be seen in Fig. 7.

This peculiarity is very different from the properties of the Talbot effect discussed in the literature for slit systems. For example, Berry & Klein (1996) have discovered the fractional Talbot effect and even the fractal Talbot effect. The fractional Talbot effect arises at distances $mz_T/2n$ where m and n are integers. The main series corresponds to $m = 1$. This series was considered by Kohn (2016) for a finite periodic system of point sources.

It was shown that due to special phase relations the periodic system of point sources creates periodic intensity distributions at distances $z_T/2n$ with period p/n. The central peak is always located between the positions of the sources. This property is not a Talbot effect and may be called a resonance when many rays interfere with the same phases, *i.e.* constructively. This resonance region covers the distance interval from zero to $z_T/4$. Then other intervals can be obtained from the symmetry rules of the Talbot effect based on the Fourier analysis which is discussed above.

We have found that the reason for this peculiarity is the fact that the wavefunction of radiation inside the peaks is complex with a variable phase. We repeat the calculation with a new initial wavefunction that has the same modulus but zero phase. The result of the calculation is shown in Fig. 8. Now the image satisfies all symmetry rules discussed above. The strong peaks at a distance of 2.3 mm disappear. However, the fractional Talbot effect is not completely revealed. This may be due to the existence of small side peaks near the central peak.

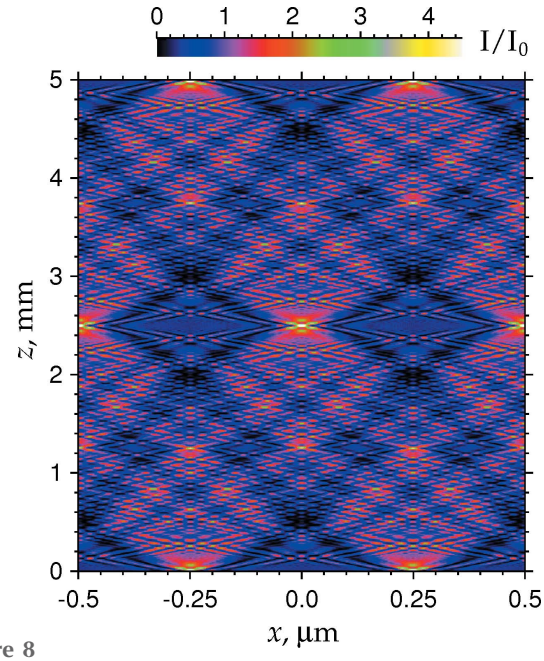

Figure 8
X-ray beam intensity distribution behind the photonic crystal within the Talbot period for the case of a wavefunction with initial modulus and zero phase.

It is of interest that an image similar to that shown in Fig. 6 was calculated by Berry & Bodenschatz (1999) and is shown in the Fig. 2(*c*) of their paper. The authors considered a special case of a sinusoidal phase grating and obtained a similar peculiarity. In our case the wavefunction was calculated in the process of transmission through a photonic crystal.

Finally we conclude that our method of calculation of X-ray beam transmission through a photonic crystal and subsequent propagation in free space behind the crystal is rather effective and allows us to analyse the effect of channeling the X-ray beam in a two-dimensional photonic crystal of complex structure.

References

Authier, A. (2005). *Dynamical Theory of X-ray Diffraction*, 3rd ed. Oxford University Press.
Berry, M. V. & Bodenschatz, E. (1999). *J. Mod. Opt.* **46**, 349–365.
Berry, M. V. & Klein, S. (1996). *J. Mod. Opt.* **43**, 2139–2164.
Bosak, A., Snigireva, I., Napolskii, K. S. & Snigirev, A. (2010). *Adv. Mater.* **22**, 3256–3259.
Byelov, D. V., Meijer, J.-M., Snigireva, I., Snigirev, A., Rossi, L., van den Pol, E., Kuijk, A., Philipse, A., Imhof, A., van Blaaderen, A., Vroege, G. J. & Petukhov, A. (2013). *RSC Adv.* **3**, 15670–15677.
Drakopoulos, M., Snigirev, A., Snigireva, I. & Schilling, J. (2005). *Appl. Phys. Lett.* **86**, 014102.
Goodman, P. & Moodie, A. F. (1974). *Acta Cryst.* A**30**, 280–290.
Gulden, J., Yefanov, O. M., Mancuso, A. P., Abramova, V. V., Hilhorst, J., Byelov, D., Snigireva, I., Snigirev, A., Petukhov, A. V. & Vartanyants, I. A. (2010). *Phys. Rev. B*, **81**, 224105.
Klimonsky, S. O., Abramova, V. V., Sinitskii, A. S. & Tretyakov, Yu. D. (2011). *Russ. Chem. Rev.* **80**, 1191–1207.
Kohn, V. G. (2002). *JETP Lett.* **76**, 600–603.
Kohn, V. G. (2003). *J. Exp. Theor. Phys.* **97**, 204–215.
Kohn, V. G. (2013). *Refraction index*, http://xray-optics.ucoz.ru/js-pro/cir-pro.htm.
Kohn, V. G. (2016). *J. Synch. Investig.* **10**, 698–704.
Kohn, V. G., Argunova, T. S. & Je, J. H. (2010). *J. Phys. D*, **43**, 442002.
Kohn, V., Snigireva, I. & Snigirev, A. (2003). *Opt. Commun.* **216**, 247–260.
Kohn, V. G., Snigireva, I. & Snigirev, A. (2014). *J. Synchrotron Rad.* **21**, 729–735.
Kohn, V. G. & Tsvigun, N. V. (2014). *Crystallogr. Rep.* **59**, 1–5.
Lengeler, B., Schroer, C., Tümmler, J., Benner, B., Richwin, M., Snigirev, A., Snigireva, I. & Drakopoulos, M. (1999). *J. Synchrotron Rad.* **6**, 1153–1167.
Macquart, Ph., Bridou, F. & Pardo, B. (1991). *Thin Solid Films*, **203**, 77–86.
Meijer, J. M., Hagemans, F., Rossi, L., Byelov, D. V., Castillo, S. I., Snigirev, A., Snigireva, I., Philipse, A. P. & Petukhov, A. V. (2012). *Langmuir*, **28**, 7631–7638.
Snigirev, A., Kohn, V., Snigireva, I. & Lengeler, B. (1996). *Nature (London)*, **384**, 49–51.
Snigirev, A., Snigireva, I., Kohn, V., Kuznetsov, S. & Schelokov, I. (1995). *Rev. Sci. Instrum.* **66**, 5486–5492.
Snigireva, I. & Snigirev, A. (2013). *J. Phys. Conf. Ser.* **463**, 012044.
Talbot, H. F. (1836). *Philos. Mag.* **9**, 401–407.